

IceCube Search for High-Energy Neutrino Emission from TeV Pulsar Wind Nebulae

M. G. AARTSEN,¹⁶ M. ACKERMANN,⁵⁵ J. ADAMS,¹⁶ J. A. AGUILAR,¹² M. AHLERS,²⁰ M. AHRENS,⁴⁶ C. ALISPACH,²⁶
K. ANDEEN,³⁷ T. ANDERSON,⁵² I. ANSEAU,¹² G. ANTON,²⁴ C. ARGÜELLES,¹⁴ J. AUFFENBERG,¹ S. AXANI,¹⁴
H. BAGHERPOUR,¹⁶ X. BAI,⁴³ A. BALAGOPAL V.,²⁹ A. BARBANO,²⁶ S. W. BARWICK,²⁸ B. BASTIAN,⁵⁵ V. BAUM,³⁶
S. BAUR,¹² R. BAY,⁸ J. J. BEATTY,^{18,19} K.-H. BECKER,⁵⁴ J. BECKER TJUS,¹¹ S. BENZVI,⁴⁵ D. BERLEY,¹⁷ E. BERNARDINI,⁵⁵
D. Z. BESSON,³⁰ G. BINDER,^{8,9} D. BINDIG,⁵⁴ E. BLAUFUSS,¹⁷ S. BLOT,⁵⁵ C. BOHM,⁴⁶ S. BÖSER,³⁶ O. BOTNER,⁵³
J. BÖTTCHER,¹ E. BOURBEAU,²⁰ J. BOURBEAU,³⁵ F. BRADASCIO,⁵⁵ J. BRAUN,³⁵ S. BRON,²⁶ J. BROSTEAN-KAISER,⁵⁵
A. BURGMAN,⁵³ J. BUSCHER,¹ R. S. BUSSE,³⁸ T. CARVER,²⁶ C. CHEN,⁶ E. CHEUNG,¹⁷ D. CHIRKIN,³⁵ S. CHOI,⁴⁸
B. A. CLARK,²² K. CLARK,³¹ L. CLASSEN,³⁸ A. COLEMAN,³⁹ G. H. COLLIN,¹⁴ J. M. CONRAD,¹⁴ P. COPPIN,¹³ P. CORREA,¹³
D. F. COWEN,^{51,52} R. CROSS,⁴⁵ P. DAVE,⁶ C. DE CLERCQ,¹³ J. J. DELAUNAY,⁵² H. DEMBINSKI,³⁹ K. DEOSKAR,⁴⁶
S. DE RIDDER,²⁷ P. DESIATI,³⁵ K. D. DE VRIES,¹³ G. DE WASSEIGE,¹³ M. DE WIT,¹⁰ T. DEYOUNG,²² A. DIAZ,¹⁴
J. C. DÍAZ-VÉLEZ,³⁵ H. DUJMOVIC,²⁹ M. DUNKMAN,⁵² E. DVORAK,⁴³ B. EBERHARDT,³⁵ T. EHRHARDT,³⁶ P. ELLER,⁵²
R. ENGEL,²⁹ P. A. EVENSON,³⁹ S. FAHEY,³⁵ A. R. FAZELY,⁷ J. FELDE,¹⁷ K. FILIMONOV,⁸ C. FINLEY,⁴⁶ D. FOX,⁵¹
A. FRANCKOWIAK,⁵⁵ E. FRIEDMAN,¹⁷ A. FRITZ,³⁶ T. K. GAISSER,³⁹ J. GALLAGHER,³⁴ E. GANSTER,¹ S. GARRAPPA,⁵⁵
L. GERHARDT,⁹ K. GHORBANI,³⁵ T. GLAUCH,²⁵ T. GLÜSENKAMP,²⁴ A. GOLDSCHMIDT,⁹ J. G. GONZALEZ,³⁹ D. GRANT,²²
T. GRÉGOIRE,⁵² Z. GRIFFITH,³⁵ S. GRISWOLD,⁴⁵ M. GÜNDER,¹ M. GÜNDÜZ,¹¹ C. HAACK,¹ A. HALLGREN,⁵³ R. HALLIDAY,²²
L. HALVE,¹ F. HALZEN,³⁵ K. HANSON,³⁵ A. HAUNGS,²⁹ D. HEBECKER,¹⁰ D. HEEREMAN,¹² P. HEIX,¹ K. HELBING,⁵⁴
R. HELLAUER,¹⁷ F. HENNINGSEN,²⁵ S. HICKFORD,⁵⁴ J. HIGNIGHT,²³ G. C. HILL,² K. D. HOFFMAN,¹⁷ R. HOFFMANN,⁵⁴
T. HOINKA,²¹ B. HOKANSON-FASIG,³⁵ K. HOSHINA,³⁵ F. HUANG,⁵² M. HUBER,²⁵ T. HUBER,^{29,55} K. HULTQVIST,⁴⁶
M. HÜNNEFELD,²¹ R. HUSSAIN,³⁵ S. IN,⁴⁸ N. IOVINE,¹² A. ISHIHARA,¹⁵ M. JANSSON,⁴⁶ G. S. JAPARIDZE,⁵ M. JEONG,⁴⁸
K. JERO,³⁵ B. J. P. JONES,⁴ F. JONSKE,¹ R. JOPPE,¹ D. KANG,²⁹ W. KANG,⁴⁸ A. KAPPES,³⁸ D. KAPPESSER,³⁶ T. KARG,⁵⁵
M. KARL,²⁵ A. KARLE,³⁵ U. KATZ,²⁴ M. KAUER,³⁵ M. KELLERMANN,¹ J. L. KELLEY,³⁵ A. KHEIRANDISH,⁵² J. KIM,⁴⁸
T. KINTSCHER,⁵⁵ J. KIRYLUK,⁴⁷ T. KITTLER,²⁴ S. R. KLEIN,^{8,9} R. KOIRALA,³⁹ H. KOLANOSKI,¹⁰ L. KÖPKE,³⁶ C. KOPPER,²²
S. KOPPER,⁵⁰ D. J. KOSKINEN,²⁰ M. KOWALSKI,^{10,55} K. KRINGS,²⁵ G. KRÜCKL,³⁶ N. KULACZ,²³ N. KURAHASHI,⁴²
A. KYRIACOU,² J. L. LANFRANCHI,⁵² M. J. LARSON,¹⁷ F. LAUBER,⁵⁴ J. P. LAZAR,³⁵ K. LEONARD,³⁵ A. LESZCZYŃSKA,²⁹
Q. R. LIU,³⁵ E. LOHFINK,³⁶ C. J. LOZANO MARISCAL,³⁸ L. LU,¹⁵ F. LUCARELLI,²⁶ A. LUDWIG,³² J. LÜNEMANN,¹³
W. LUSZCZAK,³⁵ Y. LYU,^{8,9} W. Y. MA,⁵⁵ J. MADSEN,⁴⁴ G. MAGGI,¹³ K. B. M. MAHN,²² Y. MAKINO,¹⁵ P. MALLIK,¹
K. MALLOT,³⁵ S. MANCINA,³⁵ I. C. MARIŞ,¹² R. MARUYAMA,⁴⁰ K. MASE,¹⁵ R. MAUNU,¹⁷ F. McNALLY,³³ K. MEAGHER,³⁵
M. MEDICI,²⁰ A. MEDINA,¹⁹ M. MEIER,²¹ S. MEIGHEN-BERGER,²⁵ G. MERINO,³⁵ T. MEURES,¹² J. MICALLEF,²²
D. MOCKLER,¹² G. MOMENTÉ,³⁶ T. MONTARULI,²⁶ R. W. MOORE,²³ R. MORSE,³⁵ M. MOULAI,¹⁴ P. MUTH,¹ R. NAGAI,¹⁵
U. NAUMANN,⁵⁴ G. NEER,²² L. V. NGUYN,²² H. NIEDERHAUSEN,²⁵ M. U. NISA,²² S. C. NOWICKI,²² D. R. NYGREN,⁹
A. OBERTACKE POLLMANN,⁵⁴ M. OEHLER,²⁹ A. OLIVAS,¹⁷ A. O'MURCHADHA,¹² E. O'SULLIVAN,⁴⁶ T. PALCZEWSKI,^{8,9}
H. PANDYA,³⁹ D. V. PANKOVA,⁵² N. PARK,³⁵ P. PEIFFER,³⁶ C. PÉREZ DE LOS HEROS,⁵³ S. PHILIPPEN,¹ D. PIELOTH,²¹
S. PIEPER,⁵⁴ E. PINAT,¹² A. PIZZUTO,³⁵ M. PLUM,³⁷ A. PORCELLI,²⁷ P. B. PRICE,⁸ G. T. PRZYBYLSKI,⁹ C. RAAB,¹²
A. RAISSI,¹⁶ M. RAMEEZ,²⁰ L. RAUCH,⁵⁵ K. RAWLINS,³ I. C. REA,²⁵ A. REHMAN,³⁹ R. REIMANN,¹ B. RELETHFORD,⁴²
M. RENSCHLER,²⁹ G. RENZI,¹² E. RESCONI,²⁵ W. RHODE,²¹ M. RICHMAN,⁴² S. ROBERTSON,⁹ M. RONGEN,¹ C. ROTT,⁴⁸
T. RUHE,²¹ D. RYCKBOSCH,²⁷ D. RYSEWYK CANTU,²² I. SAFA,³⁵ S. E. SANCHEZ HERRERA,²² A. SANDROCK,²¹
J. SANDROOS,³⁶ M. SANTANDER,⁵⁰ S. SARKAR,⁴¹ S. SARKAR,²³ K. SATALECKA,⁵⁵ M. SCHAUFEL,¹ H. SCHIELER,²⁹
P. SCHLUNDER,²¹ T. SCHMIDT,¹⁷ A. SCHNEIDER,³⁵ J. SCHNEIDER,²⁴ F. G. SCHRÖDER,^{29,39} L. SCHUMACHER,¹ S. SCLAFANI,⁴²
D. SECKEL,³⁹ S. SEUNARINE,⁴⁴ S. SHEFALI,¹ M. SILVA,³⁵ R. SNIHUR,³⁵ J. SOEDINGREKSO,²¹ D. SOLDIN,³⁹ M. SONG,¹⁷
G. M. SPICZAK,⁴⁴ C. SPIERING,⁵⁵ J. STACHURSKA,⁵⁵ M. STAMATIKOS,¹⁹ T. STANEV,³⁹ R. STEIN,⁵⁵ J. STETTNER,¹
A. STEUER,³⁶ T. STEZELBERGER,⁹ R. G. STOKSTAD,⁹ A. STÖSSL,¹⁵ N. L. STROTJOHANN,⁵⁵ T. STÜRWARD,¹ T. STUTTARD,²⁰
G. W. SULLIVAN,¹⁷ I. TABOADA,⁶ F. TENHOLT,¹¹ S. TER-ANTONYAN,⁷ A. TERLIUK,⁵⁵ S. TILAV,³⁹ K. TOLLEFSON,²²
L. TOMANKOVA,¹¹ C. TÖNNIS,⁴⁹ S. TOSCANO,¹² D. TOSI,³⁵ A. TRETTIN,⁵⁵ M. TSELENGIDOU,²⁴ C. F. TUNG,⁶
A. TURCATI,²⁵ R. TURCOTTE,²⁹ C. F. TURLEY,⁵² B. TY,³⁵ E. UNGER,⁵³ M. A. UNLAND ELORRIETA,³⁸ M. USNER,⁵⁵
J. VANDENBROUCKE,³⁵ W. VAN DRIESSCHE,²⁷ D. VAN ELJK,³⁵ N. VAN EIJNDHOVEN,¹³ J. VAN SANTEN,⁵⁵ S. VERPOEST,²⁷
M. VRAEGHE,²⁷ C. WALCK,⁴⁶ A. WALLACE,² M. WALLRAFF,¹ N. WANDKOWSKY,³⁵ T. B. WATSON,⁴ C. WEAVER,²³
A. WEINDL,²⁹ M. J. WEISS,⁵² J. WELDERT,³⁶ C. WENDT,³⁵ J. WERTHEBACH,³⁵ B. J. WHELAN,² N. WHITEHORN,³²
K. WIEBE,³⁶ C. H. WIEBUSCH,¹ L. WILLE,³⁵ D. R. WILLIAMS,⁵⁰ L. WILLS,⁴² M. WOLF,²⁵ J. WOOD,³⁵ T. R. WOOD,²³
K. WOSCHNAGG,⁸ G. WREDE,²⁴ D. L. XU,³⁵ X. W. XU,⁷ Y. XU,⁴⁷ J. P. YANEZ,²³ G. YODH,^{28,*} S. YOSHIDA,¹⁵ T. YUAN,³⁵
AND M. ZÖCKLEIN¹

ICECUBE COLLABORATION

- ¹*III. Physikalisches Institut, RWTH Aachen University, D-52056 Aachen, Germany*
- ²*Department of Physics, University of Adelaide, Adelaide, 5005, Australia*
- ³*Dept. of Physics and Astronomy, University of Alaska Anchorage, 3211 Providence Dr., Anchorage, AK 99508, USA*
- ⁴*Dept. of Physics, University of Texas at Arlington, 502 Yates St., Science Hall Rm 108, Box 19059, Arlington, TX 76019, USA*
- ⁵*CTSPS, Clark-Atlanta University, Atlanta, GA 30314, USA*
- ⁶*School of Physics and Center for Relativistic Astrophysics, Georgia Institute of Technology, Atlanta, GA 30332, USA*
- ⁷*Dept. of Physics, Southern University, Baton Rouge, LA 70813, USA*
- ⁸*Dept. of Physics, University of California, Berkeley, CA 94720, USA*
- ⁹*Lawrence Berkeley National Laboratory, Berkeley, CA 94720, USA*
- ¹⁰*Institut für Physik, Humboldt-Universität zu Berlin, D-12489 Berlin, Germany*
- ¹¹*Fakultät für Physik & Astronomie, Ruhr-Universität Bochum, D-44780 Bochum, Germany*
- ¹²*Université Libre de Bruxelles, Science Faculty CP230, B-1050 Brussels, Belgium*
- ¹³*Vrije Universiteit Brussel (VUB), Dienst ELEM, B-1050 Brussels, Belgium*
- ¹⁴*Dept. of Physics, Massachusetts Institute of Technology, Cambridge, MA 02139, USA*
- ¹⁵*Dept. of Physics and Institute for Global Prominent Research, Chiba University, Chiba 263-8522, Japan*
- ¹⁶*Dept. of Physics and Astronomy, University of Canterbury, Private Bag 4800, Christchurch, New Zealand*
- ¹⁷*Dept. of Physics, University of Maryland, College Park, MD 20742, USA*
- ¹⁸*Dept. of Astronomy, Ohio State University, Columbus, OH 43210, USA*
- ¹⁹*Dept. of Physics and Center for Cosmology and Astro-Particle Physics, Ohio State University, Columbus, OH 43210, USA*
- ²⁰*Niels Bohr Institute, University of Copenhagen, DK-2100 Copenhagen, Denmark*
- ²¹*Dept. of Physics, TU Dortmund University, D-44221 Dortmund, Germany*
- ²²*Dept. of Physics and Astronomy, Michigan State University, East Lansing, MI 48824, USA*
- ²³*Dept. of Physics, University of Alberta, Edmonton, Alberta, Canada T6G 2E1*
- ²⁴*Erlangen Centre for Astroparticle Physics, Friedrich-Alexander-Universität Erlangen-Nürnberg, D-91058 Erlangen, Germany*
- ²⁵*Physik-department, Technische Universität München, D-85748 Garching, Germany*
- ²⁶*Département de physique nucléaire et corpusculaire, Université de Genève, CH-1211 Genève, Switzerland*
- ²⁷*Dept. of Physics and Astronomy, University of Gent, B-9000 Gent, Belgium*
- ²⁸*Dept. of Physics and Astronomy, University of California, Irvine, CA 92697, USA*
- ²⁹*Karlsruhe Institute of Technology, Institut für Kernphysik, D-76021 Karlsruhe, Germany*
- ³⁰*Dept. of Physics and Astronomy, University of Kansas, Lawrence, KS 66045, USA*
- ³¹*SNOLAB, 1039 Regional Road 24, Creighton Mine 9, Lively, ON, Canada P3Y 1N2*
- ³²*Department of Physics and Astronomy, UCLA, Los Angeles, CA 90095, USA*
- ³³*Department of Physics, Mercer University, Macon, GA 31207-0001, USA*
- ³⁴*Dept. of Astronomy, University of Wisconsin, Madison, WI 53706, USA*
- ³⁵*Dept. of Physics and Wisconsin IceCube Particle Astrophysics Center, University of Wisconsin, Madison, WI 53706, USA*
- ³⁶*Institute of Physics, University of Mainz, Staudinger Weg 7, D-55099 Mainz, Germany*
- ³⁷*Department of Physics, Marquette University, Milwaukee, WI, 53201, USA*
- ³⁸*Institut für Kernphysik, Westfälische Wilhelms-Universität Münster, D-48149 Münster, Germany*
- ³⁹*Bartol Research Institute and Dept. of Physics and Astronomy, University of Delaware, Newark, DE 19716, USA*
- ⁴⁰*Dept. of Physics, Yale University, New Haven, CT 06520, USA*
- ⁴¹*Dept. of Physics, University of Oxford, Parks Road, Oxford OX1 3PU, UK*
- ⁴²*Dept. of Physics, Drexel University, 3141 Chestnut Street, Philadelphia, PA 19104, USA*
- ⁴³*Physics Department, South Dakota School of Mines and Technology, Rapid City, SD 57701, USA*
- ⁴⁴*Dept. of Physics, University of Wisconsin, River Falls, WI 54022, USA*
- ⁴⁵*Dept. of Physics and Astronomy, University of Rochester, Rochester, NY 14627, USA*
- ⁴⁶*Oskar Klein Centre and Dept. of Physics, Stockholm University, SE-10691 Stockholm, Sweden*
- ⁴⁷*Dept. of Physics and Astronomy, Stony Brook University, Stony Brook, NY 11794-3800, USA*
- ⁴⁸*Dept. of Physics, Sungkyunkwan University, Suwon 16419, Korea*
- ⁴⁹*Institute of Basic Science, Sungkyunkwan University, Suwon 16419, Korea*
- ⁵⁰*Dept. of Physics and Astronomy, University of Alabama, Tuscaloosa, AL 35487, USA*
- ⁵¹*Dept. of Astronomy and Astrophysics, Pennsylvania State University, University Park, PA 16802, USA*
- ⁵²*Dept. of Physics, Pennsylvania State University, University Park, PA 16802, USA*
- ⁵³*Dept. of Physics and Astronomy, Uppsala University, Box 516, S-75120 Uppsala, Sweden*
- ⁵⁴*Dept. of Physics, University of Wuppertal, D-42119 Wuppertal, Germany*
- ⁵⁵*DESY, D-15738 Zeuthen, Germany*

Submitted to ApJ

ABSTRACT

Pulsar wind nebulae (PWNe) are the main gamma-ray emitters in the Galactic plane. They are diffuse nebulae that emit nonthermal radiation. Pulsar winds, relativistic magnetized outflows from the central star, shocked in the ambient medium produce a multiwavelength emission from the radio through gamma rays. Although the leptonic scenario is able to explain most PWNe emission, a hadronic contribution cannot be excluded. A possible hadronic contribution to the high-energy gamma-ray emission inevitably leads to the production of neutrinos. Using 9.5 yr of all-sky IceCube data, we report results from a stacking analysis to search for neutrino emission from 35 PWNe that are high-energy gamma-ray emitters. In the absence of any significant correlation, we set upper limits on the total neutrino emission from those PWNe and constraints on hadronic spectral components.

1. INTRODUCTION

Galactic cosmic rays (CRs) are believed to reach energies of at least several PeV, the "knee" in the CR spectrum. Their interactions should generate gamma rays and neutrinos from the decay of secondary pions reaching hundreds of TeV. Because high-energy gamma rays can also originate in leptonic scenarios, the smoking gun for the identification of a Galactic cosmic accelerator relies on identifying a high-energy neutrino source.

The observation of high-energy neutrinos of astrophysical origin with IceCube (Aartsen et al. 2013a, 2014a) opened a new front in the search for Galactic CR accelerators. Since the discovery, IceCube has conducted analyses searching for the sources of cosmic neutrinos. Potential sources in the Galaxy are pre-identified from the catalogs of high-energy gamma-ray emitters in the Galaxy as high-energy gamma rays are supposed to be accompanied by their neutrino counterparts, if the sources are hadronic. In an early survey of the very-high-energy (VHE) gamma rays (100 GeV - 100 TeV) sky by Milagro (Abdo et al. 2007), a handful of sources were identified as the brightest objects after the Crab Nebula. Early predictions hinted at the possibility of identifying these sources within a few years of IceCube operation (Halzen et al. 2008; Gonzalez-Garcia et al. 2009). Further observations by Milagro, together with other imaging atmospheric Cerenkov telescopes (IACTs) and water Cerenkov telescopes, surveys by the High Energy Stereoscopic System (H.E.S.S.; Abdalla et al. 2018) and the High Altitude Water Cherenkov (HAWC; Abeysekara et al. 2017) for instance, provided a better and more comprehensive view of the Galactic plane at high energies. Interestingly, the majority of these objects were found to be pulsar wind nebulae (PWNe).

PWNe are diffuse nebulae confined inside supernova remnants (SNR) that are powered by pulsar winds gen-

erated by the highly spinning and magnetized pulsars in the center. According to observations mentioned above, PWNe are the most numerous TeV gamma-ray emitters in the Milky Way.

The photon emission of PWNe is believed to be mainly from relativistic electron-positron pairs, which are the primary components of the pulsar winds. These magnetized winds are powered by the rotational energy of the central pulsars. In this leptonic scenario, the low-energy emission (radio, optical, and X-ray) is dominated by synchrotron emission of relativistic leptons, and the inverse Compton scattering (ICS) of synchrotron photons becomes dominant at high energies (TeV). The leptonic scenario can accommodate the photon spectrum from radio wavelengths to TeV (Kargaltsev & Pavlov 2010). However, the presence of hadrons coexisting with leptons is still uncertain and to date cannot be excluded by either theory or observation. The hadronic mechanism was first discussed in the context of the VHE gamma-ray emission of the Crab Nebula, where protons accelerated in the outer gap of the pulsar interacting with the nebula (Cheng et al. 1990) and heavy nuclei accelerated in the pulsar magnetosphere interacting with soft photons (Bednarek & Protheroe 1997). In addition, neutrino emission from PWNe has been studied for CR acceleration at the termination shocks followed by interactions in the source region with photons or nuclei (see, e.g., Guetta & Amato 2003; Amato et al. 2003; Bednarek 2003; Lemoine et al. 2015; Palma et al. 2017). Even minor contamination of ions at the termination shock would lead to considerable amount of energy contents released in hadrons. In such scenario, a neutrino flux is expected due to hadronuclear interactions (see Amato & Arons 2006, for details).

VHE gamma-ray emission from PWNe and the possibility of their hadronic origin render PWNe of interest to IceCube. Previous IceCube searches have set upper limits on the neutrino flux from a list of individual PWNe (Aartsen et al. 2013b, 2014b, 2017a) and also a stack-

* Deceased

ing search on nine PWNe using 7 yr of data has been performed (Aartsen et al. 2017b). Assuming part of the TeV gamma-ray emission from PWNe is hadronic, we report a stacking analysis on 35 TeV PWNe using 9.5 yr of IceCube all-sky neutrino data.

2. SEARCH FOR NEUTRINO EMISSION

2.1. Source Selection

In astrophysical beam dumps, when accelerated CRs interact with matter or ambient radiation, both neutral and charged pion secondaries are produced. While charged pions decay into high-energy neutrinos, neutral pions decay and create a flux of high-energy gamma rays. Therefore, in the context of multimessenger connection, high-energy neutrinos are inevitably accompanied by pionic gamma rays. PWNe with detected VHE gamma rays are of interest in the context of multimessenger astronomy, for possible hadronic origin in addition to photons scattered to higher energies via ICS. Therefore, in this search, we consider sources identified as PWNe with gamma-ray emission higher than 1 TeV. These are sources observed by the high-energy gamma-ray telescopes HAWC, H.E.S.S., Major Atmospheric Gamma-Ray Imaging Cherenkov (MAGIC), and Very Energetic Radiation Imaging Telescope Array System (VERITAS), which currently observe the highest energy photons. The associated pulsars of these PWNe are listed in the Australia Telescope National Facility (ATNF) catalog (Manchester et al. 2005). The source list is presented in Table 3 along with detailed information on the position, extension, age, period, and gamma-ray spectrum of each source.

2.2. Method

Here, we use an unbinned maximum likelihood to perform a stacking search for neutrino emission from TeV PWNe. This analysis seeks a significant excess of neutrino events (signal) from directions interested above the background of atmospheric neutrinos and diffuse astrophysical neutrinos. The method is described in Braun et al. (2008). Stacking potential sources together is an effective way to improve the sensitivity of a search for neutrino sources (Achterberg et al. 2006). The unbinned likelihood function for a stacking search is defined as

$$\mathcal{L}(n_s, \gamma_s) = \prod_i^N \left(\frac{n_s}{N} \sum_j^M \omega_j S_i^j + \left(1 - \frac{n_s}{N}\right) B_i \right), \quad (1)$$

where n_s is the number of signal events and γ_s is the spectral index of a power-law spectrum. N is the total number of neutrino events and M is the number of sources. S_i^j is the signal probability density function

(PDF), which corresponds to the i th event with respect to the j th source. The normalized weight, ω_j , determines the relative normalization of the signal PDF from source j . Finally, B_i is the background PDF.

The PDFs are composed of the spatial part and the energy part, therefore, for the signal $S_i^j = S^s(x_j, x_i, \sigma_{ij}) \times S^E(E_i, \gamma_s)$ and similarly for the background $B_i = 1/(2\pi)B^\delta(\delta_i) \times B^E(E_i)$. x_j is the location of source j ; x_i , δ_i and E_i are the reconstructed location, declination and energy of event i . For S_i^j , the spatial clustering of signal events is modeled as a two-dimensional Gaussian distribution. The width of the spatial PDF, σ_{ij} , representing the effective angular uncertainty of event σ_i and the angular extension of source σ_j , is defined as $\sigma_{ij} = (\sigma_i^2 + \sigma_j^2)^{1/2}$. An event energy proxy is used to separate a potential hard-spectrum signal from the softer spectrum background. We model the signal spectrum as an unbroken power-law spectrum, $E^{-\gamma_s}$, where the spectral index, γ_s , is assumed to have a value between 1 and 4. In order to avoid bias, we set the spectral index γ_s as a generic parameter for all sources instead of using the measured index for each source from gamma-ray observations. For B_i , it is constructed from binning the experimental data in the reconstructed declination and energy. $1/2\pi$ arises due to IceCube, located at the South Pole, has a uniform acceptance in right ascension. Since we search for an excess of neutrino events from preassigned source locations, the background is estimated by randomizing the right ascensions of the experimental data sample to remove any correlation with sources being tested. The likelihood is maximized for two parameters: number of signal events, n_s , and the spectral index, γ_s . The null hypothesis presumes no signal-like event, i.e., $n_s = 0$. The test statistic (TS) is defined by a maximal log-likelihood ratio, $\text{TS} = 2 \log[\mathcal{L}(\hat{n}_s, \hat{\gamma}_s)/\mathcal{L}(n_s = 0)]$ in which \hat{n}_s and $\hat{\gamma}_s$ are the best-fitting values. A distribution of background TS values approximately following χ^2 distribution can be generated after randomizing the neutrino map many times. The actual data can give the observed TS. The p -value, which represents the probability that the background being able to create a TS the same or larger than the observed TS, is defined as the fraction of TS larger than the observed one in the total background TS distribution.

2.3. Weighting

The weight term ω_j is composed of two terms a "model" term $\omega_{j,\text{model}}$ and a detector acceptance term $\omega_{j,\text{det}}$, i.e.,

$$\omega_j = \frac{\omega_{j,\text{model}} \cdot \omega_{j,\text{det}}}{\sum_j^M \omega_{j,\text{model}} \cdot \omega_{j,\text{det}}}. \quad (2)$$

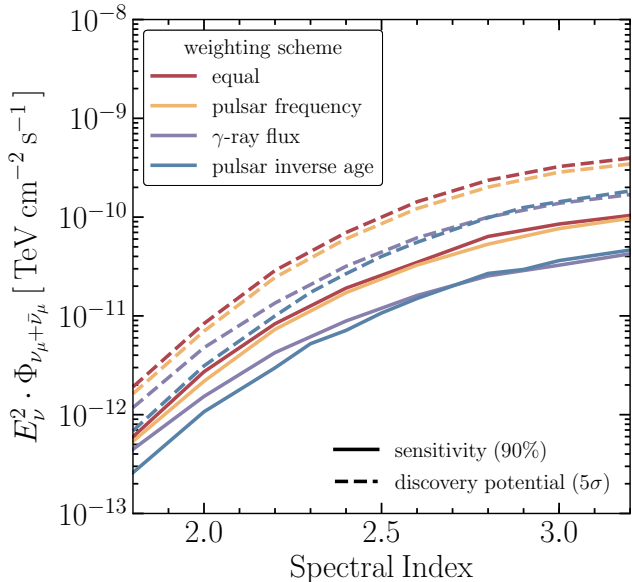


Figure 1. Sensitivities (90% CL) and 5σ discovery potentials of different weighting schemes as a function of spectral index for an unbroken power-law spectrum.

The detector acceptance term $\omega_{j,\text{det}}$ can be determined by the spectrum and the effective area of the detector for an event from the direction of the source $\omega_{j,\text{det}} \propto \int_{E_{\text{min}}}^{E_{\text{max}}} E^{-\gamma_s} A_{\text{eff}}(\theta_j, E) dE$, where θ_j is the zenith angle of source j . About the unknown model term, $\omega_{j,\text{model}}$, theoretical or observational arguments can be used in the weights applied to each source in order to test a specific hypothesis, such as correlation of neutrino emission with a particular property of a source. In a generic astrophysical beam dump, the production rate of neutrinos depends on the matter density and injection power of accelerated CRs. Furthermore, the capability of an accelerator to reach very high energies depends on how strongly it can confine the particles, as stated by the Hillas criterion (Hillas 1984). In the following we will adopt the main characteristics of PWNe that could attribute to these criteria and will test four distinct hypotheses by incorporating different weighting schemes according to these properties:

Equal weighting In this scheme, $\omega_{j,\text{model}} = 1$, which assigns the neutrino emission of each source the same probability. Therefore, no preference is given to any source and they are treated equally.

Gamma-ray flux weighting This case assumes that a plausible high-energy neutrino emission is directly proportional to the high-energy gamma-ray emission from each source. If this assumption is true, this basically means that the observed high-energy gamma rays are either partially or completely of hadronic origin. Here,

we incorporate the gamma-ray flux at 1 TeV as the weights. As indicated in Table 3, for sources in the Northern sky, spectral measurements from MAGIC and VERITAS are used; while for sources in the Southern sky, H.E.S.S. is used as it is more sensitive in this region. The HAWC observations are used for Geminga and 2HWC J0700+143.

Pulsar spin frequency weighting- The energy carried by the pulsar wind for the acceleration is taken from the rotational energy of the pulsar as it emits radiation, which results in the spin-down of the pulsar (Gaensler & Slane 2006). Faster spinning pulsars are more energetic, and are considered as candidate sources of ultra-high-energy CRs, see, for example Bednarek & Protheroe (2002); Kotera et al. (2015). In addition, the acceleration time has a strong dependence on the period. Therefore, the period of the pulsar, as an important measure of how energetic the pulsar is, is used as the weight in this scheme. In this scheme, faster spinning sources are preferred.

Age weighting- The characteristic age of a pulsar is usually defined as $\tau = \frac{P}{2\dot{P}}$ where P and \dot{P} are the period and its time derivative, respectively. This parameter is used to estimate the true age of a pulsar under assumptions that the initial spin is much faster than today and the energy loss is from magnetic dipole radiation (Gaensler & Slane 2006). Following the discussion of spin frequency weighting scheme, the age of a pulsar presents another factor that may determine how energetic it is, as the age is not only dependent on the period but also on its time derivative. Given that young fast-spinning neutron star winds have been proposed as the sites for CR acceleration (Blasi et al. 2000; Bednarek 2003; Fang et al. 2016). Here, we use $1/\text{age}$ as the weight for each source. This assumption prefers younger PWNe to be more energetic emitters. This hypothesis is in accordance with the idea that young and highly magnetized pulsars are primary sources of ultra-high-energy CRS. On the other hand, this scenario may also examine the hypothesis that accelerated particles are not currently part of the pulsar wind, instead, they have been injected in the nebula at some earlier time when the pulsar was much younger and more energetic (Atoyan 1999).

2.4. Detector \mathcal{E} Data Set

The IceCube Neutrino Observatory at the South Pole has transformed a cubic kilometer of Antarctic ice into a Cerenkov detector and has been monitoring the whole sky continuously since 2008. The detector is an array of digital optical modules (DOMs) each including a photomultiplier tube and on-board read-out electronics (Ab-

basi et al. 2010, 2009). The complete configuration accomplished in 2010 is composed of 5160 DOMs arranged in 86 strings from 1450 - 2450 m below the surface in Antarctic ice (Aartsen et al. 2017d). The Cerenkov light emitted by the secondary particles produced in neutrino interactions are registered by the DOMs, and particle trajectories are determined by the arrival times of photons at the optical sensors. The number of photons observed along with their timings are used to determine the energy deposited by charged secondary particles in the detector. While IceCube is able to detect neutrinos of all flavors, long tracks resulting from muon neutrino interactions can point back to the sources with a typical angular resolution of less than 1° (Aartsen et al. 2017a).

In this analysis, we use 9.5 yr all-sky data collected by IceCube between 2008 April and 2017 November. This includes 7 yr of data already studied for neutrino point sources (Aartsen et al. 2017a) along with additional data for the period from 2015 May to 2017 November (Aartsen et al. 2017c). These 9.5 yr of data correspond to six distinct periods specified in Table 1. These periods differ in detector configuration, data-taking conditions, and event selections.

To estimate the performance of the analysis, source emission is simulated to observe the detector response. Sensitivities (90% confidence level (CL)) and discovery potentials (5σ) for different weighting scenarios discussed in Sec. 2.3 are shown in Figure 1. For simulating the neutrino emission, an unbroken power-law spectral shape is assumed. The projected sensitivity shows, as expected, that IceCube is more sensitive to sources with a harder spectrum. The difference of the sensitivities

between weighting schemes is dependent on the weight distribution, which represents how significant we assume one location is. For example, more sources in the Northern sky with higher weights imply a better sensitivity to IceCube.

3. RESULTS

We performed the unbinned likelihood analysis discussed in Sec. 2.2 for different hypotheses of neutrino emission considering equal, frequency, gamma-ray flux, and inverse age weighting. The results for these tests are presented in Table 2. The largest excess was found in the equal weighting scheme, yielding a fitted signal of 40.4 events with a p -value of 0.22, which shows no significant correlation. Therefore, the isotropic background distribution (null) hypothesis is preferred. Because none of the tests led to a significant excess of fitted signal events and the results are compatible with the null hypothesis, we set upper limits on the total flux of high-energy neutrinos from PWNe for each hypothesis. Upper limits with a 90% CL are presented for three different spectral shape assumptions in Table 2.

4. DISCUSSION

Due to the apparent isotropy of astrophysical neutrinos observed by IceCube, An extragalactic origin is expected to be predominant. However, Galactic CR accelerators are expected to contribute at a subdominant level to the observed high-energy cosmic neutrino flux. The Galactic component of the high-energy neutrino flux is constrained to $\sim 14\%$ at 1 TeV (Aartsen et al. 2017b) of the combined diffuse neutrino flux measured in Aartsen et al. (2015). The upper limit obtained in this study for neutrino emission from TeV PWNe is consistent with this limit by showing no more than $\sim 1.6\%$ contribution to the combined flux in this search. Considering the astrophysical muon neutrino flux reported (Haack & Wiebusch 2018), the contribution of neutrino emission from TeV PWNe studied here to the total neutrino flux is less than $\sim 4\%$. We note that this limit is valid within the specific assumptions of this analysis regarding the weighting and selection of the sources and should not be applied or extended to other hypotheses.

In the context of a multimessenger connection, neutrino fluxes can be related to the high-energy gamma-ray flux; see Ahlers & Murase (2014) for details. With this connection, one can use the upper limit on the neutrino flux to constrain the hadronic component of the observed high-energy gamma-ray flux. Here, we assume hadronuclear (i.e., proton-proton) interactions at the source to convert neutrino fluxes to their gamma-ray

Table 1. IceCube Data Set

Sample	Livetime	Events
	days	#
IC 40	376.36	36900
IC 59	353.58	107011
IC 79	316.05	93133
IC 86 I	332.96	136244
IC 86 II	1058.48	338590
GFU 2015-2017	989.95	571040

NOTE—The data set used in this search.

The first seven years of data, IC40-IC86 II, are the same as data used in (Aartsen et al. 2017a,b) and the latter 2.5 years, GFU 2015-2017, are discussed in (Aartsen et al. 2017c).

Table 2. Results

weighting	TS	n_s	γ	p -value	$\Phi_{\nu_\mu+\bar{\nu}_\mu}^{90\%, E^{-2.0}}$	$\Phi_{\nu_\mu+\bar{\nu}_\mu}^{90\%, E^{-2.19}}$	$\Phi_{\nu_\mu+\bar{\nu}_\mu}^{90\%, E^{-2.5}}$
Equal	0.81	40.43	3.84	23%	3.91	11.6	44.5
Frequency	0.26	18.00	3.81	38%	2.64	7.79	28.2
Flux	0.21	8.73	4.00	36%	1.74	4.57	14.9
Inverse age	0	0	-	-	1.07	2.82	10.7

NOTE—Best fits for TS, n_s and γ . The last three columns are upper limit constraints on the stacking flux with a 90% CL. The first one has a power-law spectrum $E^{-2.0}$; the second has $E^{-2.19}$, which is the measured astrophysical muon neutrino spectrum by IceCube (Haack & Wiebusch 2018) and the last column follows $E^{-2.5}$, which is the IceCube all-flavor combined neutrino spectrum (Aartsen et al. 2015). They are all normalized at 1 TeV with units $10^{-12} \text{ TeV}^{-1} \text{ cm}^{-2} \text{ s}^{-1}$.

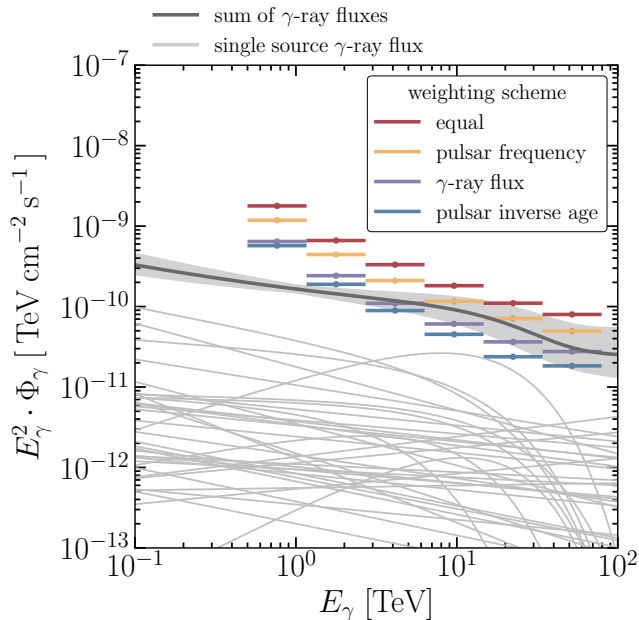


Figure 2. Light gray lines are observed gamma-ray spectra of the sources in this search, and the dark gray line is the sum of those fluxes. The total uncertainty is estimated by simply summing up the uncertainty of the flux of each source. Red, orange, purple, and blue steps show the differential upper limit on the hadronic gamma-ray emission. The upper limits are obtained by converting 90% CL differential upper limit on the neutrino flux, and each color corresponds to a given weighting method. To avoid uncertainties from extrapolation, the energy is limited to 100 TeV here.

counterparts. For protongamma interactions, one can easily adjust protonproton flux by a factor of 2, taking account the different ratio of charged to neutral pions in each process.

High-energy gamma-ray flux measurements extend to tens of TeV, while IceCube neutrinos reach energies of a few PeV. To avoid the large uncertainties in extrapolation of the high-energy gamma-ray flux, we calculate differential upper limits assuming an unbroken power-

law spectrum and convert the neutrino limits into upper limits on a hadronic gamma-ray flux at energies below 100 TeV. Figure 2 shows the differential upper limits for an E^{-2} spectrum for different hypotheses tests of this study compared to the observed cumulative flux of VHE gamma rays. As expected, the constraints are stronger at higher energies. At energies between 10 and 100 TeV, the hadronic component of the high-energy emission from these sources are constrained, if the neutrino emission is either correlated with the observed gamma-ray emission or if younger PWNe are more efficient neutrino emitters. However, if the emission is proportional to the pulsar’s frequency, upper limits are marginally at the same level of the total gamma-ray emission.

5. CONCLUSION & OUTLOOK

Galactic CRs reach energies of at least several PeV, and their interactions should generate gamma rays and neutrinos from the decay of secondary pions. Therefore, Galactic sources are expected to contribute at some level to the total high-energy cosmic neutrino flux observed by IceCube. In the initial survey of the VHE sky by Milagro (Abdo et al. 2007), where the observed gamma-ray flux in TeV was found higher than the expected leptonic emission, promising sources had been identified based on their spectra, assuming that the highest energy gamma rays are pionic. Early estimates showed that the observation of these sources were likely in the lifetime of IceCube (Halzen et al. 2008; Gonzalez-Garcia et al. 2009). Further observation of the Galactic plane by IACTs provided more insight, and updated estimates showed that IceCube would identify those sources provided that the gamma-ray fluxes did not cut off at low energies (Gonzalez-Garcia et al. 2014; Halzen et al. 2017). Meanwhile, the majority of the sources in the plane were identified to be PWNe. Leptonic scenarios are generally more favored for describing the high-energy

emission from PWNe. However, a hadronic component cannot be excluded by current observations. Hadronic interactions at the source will inevitably result in the production of neutrinos that provide the smoking gun for the presence of the hadrons.

In this study, we examined the possible neutrino emission from PWNe with TeV gamma-ray emission. Thirty-five sources were identified, and the results of the stacking searches for the high-energy neutrino emission are compatible with the isotropic arrival direction hypothesis. In the absence of a significant excess of neutrino events in the direction of these sources, we have set upper limits on the total neutrino emission and on the potential hadronic component of the high-energy gamma-ray flux.

Any evidence for presence (or absence) of the hadrons in pulsar winds would provide important clues about the mechanism of acceleration in these sources, for more details see, e.g. (Amato 2014). The so-called σ problem¹ could be solved if the majority of the pulsar wind energy is carried by hadrons and further explain how efficient acceleration of leptons is obtained in the termination shocks (Palma et al. 2017). The stacking analysis presented here found upper limits at the level of the total observed high-energy gamma-ray emission indicating that neutrino flux measurements getting close to determine the feasibility of such models.

In the future, more accurate measurement of the VHE gamma-ray flux by HAWC and coming gamma-ray observatories, such as CTA (Acharya et al. 2018) and LHAASO (Di Sciacio 2016), will shed more light on the nature of the high-energy emission from the Milky Way. From the perspective of neutrino detection, the addition of more years of data with continuous operation of IceCube will improve the sensitivity of the search for Galactic sources of cosmic neutrinos. The next step, IceCube-Gen2, a substantial expansion of IceCube, will be 10 times larger. This next-generation neutrino observatory with five times the effective area of IceCube is expected to improve the neutrino source search sensitivity by the same order (Aartsen et al. 2014c; Ahlers & Halzen 2014; Aartsen et al. 2019). With higher neutrino statistics, identifying Galactic sources will become more

promising.

ACKNOWLEDGEMENTS

The IceCube collaboration acknowledges the significant contributions to this manuscript from Ali Kheirandish and Qinrui Liu. The authors gratefully acknowledge the support from the following agencies and institutions: USA – U.S. National Science Foundation-Office of Polar Programs, U.S. National Science Foundation-Physics Division, Wisconsin Alumni Research Foundation, Center for High Throughput Computing (CHTC) at the University of Wisconsin-Madison, Open Science Grid (OSG), Extreme Science and Engineering Discovery Environment (XSEDE), U.S. Department of Energy-National Energy Research Scientific Computing Center, Particle astrophysics research computing center at the University of Maryland, Institute for Cyber-Enabled Research at Michigan State University, and Astroparticle physics computational facility at Marquette University; Belgium – Funds for Scientific Research (FRS-FNRS and FWO), FWO Odysseus and Big Science programmes, and Belgian Federal Science Policy Office (Belspo); Germany – Bundesministerium für Bildung und Forschung (BMBF), Deutsche Forschungsgemeinschaft (DFG), Helmholtz Alliance for Astroparticle Physics (HAP), Initiative and Networking Fund of the Helmholtz Association, Deutsches Elektronen Synchrotron (DESY), and High Performance Computing cluster of the RWTH Aachen; Sweden – Swedish Research Council, Swedish Polar Research Secretariat, Swedish National Infrastructure for Computing (SNIC), and Knut and Alice Wallenberg Foundation; Australia – Australian Research Council; Canada – Natural Sciences and Engineering Research Council of Canada, Calcul Québec, Compute Ontario, Canada Foundation for Innovation, WestGrid, and Compute Canada; Denmark – Villum Fonden, Danish National Research Foundation (DNRF), Carlsberg Foundation; New Zealand – Marsden Fund; Japan – Japan Society for Promotion of Science (JSPS) and Institute for Global Prominent Research (IGPR) of Chiba University; Korea – National Research Foundation of Korea (NRF); Switzerland – Swiss National Science Foundation (SNSF); United Kingdom – Department of Physics, University of Oxford.

¹ σ problem refers to the conflicting scenario in theoretical models of pulsar wind. σ presents the ratio of the wind Poynting flux to its kinetic energy flux. While theoretical models of pulsar magnetospheres and wind predict large σ , the 1D MHD simulations of PWN cannot match shock size and expansion speed at same time with high sigma.

REFERENCES

- Aartsen, M. G., et al. 2013a, *Science*, 342, 1242856
— 2013b, *Astrophys. J.*, 779, 132
— 2014a, *Phys.Rev.Lett.*, 113, 101101
— 2014b, *Astrophys. J.*, 796, 109
— 2014c, arXiv:1412.5106
— 2015, *Astrophys. J.*, 809, 98
— 2017a, *Astrophys. J.*, 835, 151
— 2017b, *Astrophys. J.*, 849, 67
— 2017c, *Astropart. Phys.*, 92, 30
— 2017d, *JINST*, 12, P03012
— 2019, arXiv:1911.02561
- Abbasi, R., et al. 2009, *Nucl. Instrum. Meth.*, A601, 294
— 2010, *Nucl. Instrum. Meth.*, A618, 139
- Abdalla, H., et al. 2018, *Astron. Astrophys.*, 612, A1
- Abdo, A. A., et al. 2007, *Astrophys. J.*, 658, L33
- Abeysekera, A. U., et al. 2017, *Astrophys. J.*, 843, 40
- Abramowski, A., et al. 2015, *Science*, 347, 406
- Acciari, V. A., et al. 2009, *Astrophys. J.*, 703, L6
— 2010, *Astrophys. J.*, 719, L69
- Acero, F., Djannati Ataï, A., Förster, A., Gallant, Y., & Renaud, M. 2012, in *Proceedings, 32nd International Cosmic Ray Conference (ICRC 2011): Beijing, China, August 11-18, 2011, Vol. 7*, 185–188
- Acharya, B. S., et al. 2018, *Science with the Cherenkov Telescope Array (WSP)*, arXiv:1709.07997
- Achterberg, A., et al. 2006, *Astropart. Phys.*, 26, 282
- Aharonian, F., et al. 2006, *Astron. Astrophys.*, 457, 899
- Ahlers, M., & Halzen, F. 2014, *Phys. Rev.*, D90, 043005
- Ahlers, M., & Murase, K. 2014, *Phys. Rev.*, D90, 023010
- Aleksić, J., et al. 2014a, *Astron. Astrophys.*, 567, L8
— 2014b, *Astron. Astrophys.*, 571, A96
- Aliu, E., et al. 2013, *Astrophys. J.*, 764, 38
— 2014a, *Astrophys. J.*, 788, 78
— 2014b, *Astrophys. J.*, 783, 16
- Amato, E. 2014, *Int. J. Mod. Phys. Conf. Ser.*, 28, 1460160
- Amato, E., & Arons, J. 2006, *Astrophys. J.*, 653, 325
- Amato, E., Guetta, D., & Blasi, P. 2003, *Astron. Astrophys.*, 402, 827
- Atoyan, A. M. 1999, *A&A*, 346, L49
- Bednarek, W. 2003, *Astron. Astrophys.*, 407, 1
- Bednarek, W., & Protheroe, R. 2002, *Astropart. Phys.*, 16, 397
- Bednarek, W., & Protheroe, R. J. 1997, *Phys. Rev. Lett.*, 79, 2616
- Blasi, P., Epstein, R. I., & Olinto, A. V. 2000, *Astrophys. J.*, 533, L123
- Braun, J., Dumm, J., De Palma, F., et al. 2008, *Astropart. Phys.*, 29, 299
- Cheng, K. S., Cheung, T., Lau, M. M., Yu, K. N., & Kwok, P. W. 1990, *J. Phys.*, G16, 1115
- Di Sciacio, G. 2016, *Nucl. Part. Phys. Proc.*, 279-281, 166
- Fang, K., Kotera, K., Murase, K., & Olinto, A. V. 2016, *JCAP*, 04, 010
- Gaensler, B. M., & Slane, P. O. 2006, *Ann. Rev. Astron. Astrophys.*, 44, 17
- Gonzalez-Garcia, M. C., Halzen, F., & Mohapatra, S. 2009, *Astropart. Phys.*, 31, 437
- Gonzalez-Garcia, M. C., Halzen, F., & Niro, V. 2014, *Astropart. Phys.*, 57-58, 39
- Guetta, D., & Amato, E. 2003, *Astropart. Phys.*, 19, 403
- Haack, C., & Wiebusch, C. 2018, *PoS, ICRC2017*, 1005
- Halzen, F., Kappes, A., & O’Murchadha, A. 2008, *Phys. Rev.*, D78, 063004
- Halzen, F., Kheirandish, A., & Niro, V. 2017, *Astropart. Phys.*, 86, 46
- Hillas, A. M. 1984, *Annual review of astronomy and astrophysics*, 22, 425
- Kargaltsev, O., & Pavlov, G. 2010, *AIP Conf. Proc.*, 1248, 25
- Kotera, K., Amato, E., & Blasi, P. 2015, *JCAP*, 08, 026
- Lemoine, M., Kotera, K., & Ptri, J. 2015, *JCAP*, 1507, 016
- Manchester, R. N., Hobbs, G. B., Teoh, A., & Hobbs, M. 2005, *Astron. J.*, 129, 1993
- Palma, I. D., Guetta, D., & Amato, E. 2017, *Astrophys. J.*, 836, 159
- Sheidaei, F., Djannati-Ata, A., & Gast, H. 2011, in *Proceedings, 32nd International Cosmic Ray Conference (ICRC 2011): Beijing, China, August 11-18, 2011, Vol. 7*, 244–247

Table 3. Sources in this search.

PWN	Pulsar	R.A.	Dec.	Extension	Period	Age	N_0	γ	Cutoff	Telescope	Ref.
		deg	deg	deg	s	kyr	$\text{TeV}^{-1} \text{cm}^{-2} \text{s}^{-1}$		TeV		
CTA1	J0007+7303	1.61	72.98	0.25	0.316	13.9	0.10	2.2	—	VERITAS	(Aliu et al. 2013)
3C 58	J0205+6449	31.38	64.85	—	0.0657	5.37	0.02	2.4	—	MAGIC	(Aleksić et al. 2014a)
Crab	B0531+21	83.63	22.01	—	0.033	1.26	3.76	2.39	14.3	HESS	(Aharonian et al. 2006)
LHA 120-N 157B	J0537-6910	84.43	-69.17	0.014	0.0161	4.93	0.13	2.8	—	HESS	(Abramowski et al. 2015)
Geminga	J0633+1746	98.12	17.37	2.0	0.237	342.0	0.37	2.23	—	HAWC	(Abeysekara et al. 2017)
2HWC J0700+143	B0656+14	105.12	14.32	1.0	0.385	111.0	0.094	2.17	—	HAWC	(Abeysekara et al. 2017)
Vela X	B0833-45	128.75	-45.6	0.59	0.089	11.3	1.21	1.35	12.27	HESS	(Abdalla et al. 2018)
HESS J1018-589B	J1016-5857	154.13	-58.98	0.15	0.107	21.0	0.084	2.2	—	HESS	(Abdalla et al. 2018)
HESS J1026-582	J1028-5819	156.66	-58.2	0.13	0.0914	90.0	0.054	1.81	—	HESS	(Abdalla et al. 2018)
SNR G292.2-00.5	J1119-6127	169.75	-61.4	0.098	0.408	1.61	0.15	2.64	—	HESS	(Abdalla et al. 2018)
HESS J1303-631	J1301-6305	195.7	-63.18	0.177	0.185	11.0	0.63	2.04	15.12	HESS	(Abdalla et al. 2018)
HESS J1356-645	J1357-6429	209.0	-64.5	0.23	0.166	7.31	0.53	2.2	—	HESS	(Abdalla et al. 2018)
Kookaburra(Rabbit)	J1418-6058	214.52	-60.98	0.108	0.111	10.3	0.34	2.26	—	HESS	(Abdalla et al. 2018)
Kookaburra(PWN)	J1420-6048	215.04	-60.76	0.081	0.0682	13.0	0.33	2.2	—	HESS	(Abdalla et al. 2018)
HESS J1458-608	J1459-6053	224.54	-60.88	0.373	0.103	64.7	0.11	1.81	—	HESS	(Abdalla et al. 2018)
MSH15-52	B1509-58	228.53	-59.16	0.15	0.151	1.56	0.69	2.05	19.2	HESS	(Abdalla et al. 2018)
SNR G327.1-01.1 ^a	-	238.65	-55.08	—	0.035	18.0	0.035	2.19	—	HESS	(Abdalla et al. 2018)
HESS J1616-508	J1617-5055	244.1	-50.9	0.232	0.0693	8.13	1.06	2.32	—	HESS	(Abdalla et al. 2018)
HESS J1632-478	J1632-4757	248.04	-47.82	0.182	0.229	240.0	0.35	2.52	—	HESS	(Abdalla et al. 2018)
HESS J1640-465	J1640-4631	250.18	-46.53	0.11	0.206	3.35	0.45	2.12	4.13	HESS	(Abdalla et al. 2018)
HESS J1708-443	B1706-44	257.05	-44.33	0.279	0.102	17.5	0.39	2.17	—	HESS	(Abdalla et al. 2018)
HESS J1718-385	J1718-3825	259.53	-38.55	0.115	0.0747	89.5	0.030	0.98	10.57	HESS	(Abdalla et al. 2018)
SNR G000.9+00.1	J1747-2809	266.85	-28.15	—	0.0521	5.31	0.084	2.4	—	HESS	(Abdalla et al. 2018)
HESS J1813-178	J1813-1749	273.4	-17.84	0.049	0.0447	5.6	0.22	1.64	7.37	HESS	(Abdalla et al. 2018)
HESS J1825-137	B1823-13	276.42	-13.84	0.461	0.101	21.4	2.56	2.15	13.57	HESS	(Abdalla et al. 2018)
HESS J1831-098	J1831-0952	277.85	-9.9	0.15	0.0673	128.0	0.11	2.1	—	HESS	(Sheidaei et al. 2011)
HESS J1833-105	J1833-1034	278.39	-10.56	—	0.0619	4.85	0.038	2.42	—	HESS	(Abdalla et al. 2018)
HESS J1837-069	J1838-0655	279.41	-6.95	0.355	0.0705	22.7	1.78	2.54	—	HESS	(Abdalla et al. 2018)

Table 3 continued

Table 3 (*continued*)

PWN	Pulsar	R.A.	Dec.	Extension	Period	Age	N_0	γ	Cutoff	Telescope	Ref.
		deg	deg	deg	s	kyr	$\text{TeV}^{-1} \text{cm}^{-2} \text{s}^{-1}$		TeV		
HESS J1846-029	J1846-0258	281.6	-2.98	—	0.327	0.73	0.067	2.41	—	HESS	(Abdalla et al. 2018)
IGR J18490-0000	J1849-0001	282.24	-0.04	0.09	0.0385	42.9	0.056	1.97	—	HESS	(Abdalla et al. 2018)
MAGIC J1857.2+0263	J1856+0245	284.3	2.63	0.1	0.0809	20.6	0.24	2.2	—	MAGIC	(Aleksić et al. 2014b)
SNR G054.1+00.3	J1930+1852	292.63	18.87	—	0.137	2.89	0.075	2.39	—	VERITAS	(Acciari et al. 2010)
MGRO J2019+37	J2021+3651	304.65	36.83	0.75	0.104	17.2	0.14	1.75	—	VERITAS	(Aliu et al. 2014a)
TeV J2032+4130	J2032+4127	308.03	41.51	0.158	0.143	201.0	0.095	2.1	—	VERITAS	(Aliu et al. 2014b)
Boomerang	J2229+6114	337.18	61.17	0.22	0.0516	10.5	0.14	2.29	—	VERITAS	(Acciari et al. 2009)

NOTE—Equatorial coordinates (J2000) of sources are from TeVCat. Ages and periods that are related to the associated pulsars are from ATNF (Manchester et al. 2005). The last two columns refer to telescopes and references that made spectrum (normalized fluxes, spectral indices, and exponential cutoff energies, if applicable) and angular extension measurements of the source. N_0 in the table shows the gamma-ray flux at 1 TeV.

^aPeriod and age are from estimation (Acero et al. 2012).